Electrical Power and Energy Systems 71 (2015) 68–76

Contents lists available at ScienceDirect

Electrical Power and Energy Systems

journal homepage: www.elsevier.com/locate/ijepes

A robust control strategy for a grid-connected multi-bus microgrid under unbalanced load conditions

Mohammad Mahdi Rezaei [a,*], Jafar Soltani [b,1]

[a] Department of Technical & Engineering, Science and Research Branch, Islamic Azad University, Tehran, Iran
[b] Department of Electrical Engineering, Khomeinishahr Branch, Islamic Azad University, Isfahan, Iran

ARTICLE INFO

Article history:
Received 10 August 2014
Received in revised form 14 January 2015
Accepted 20 February 2015
Available online 13 March 2015

Keywords:
Microgrid
Distributed generation
Unbalanced load
Symmetrical components
Lyapunov function (LF)
Sliding mode (SM) control

ABSTRACT

The increasing presence of inverter-based distributed generation (DG) units in microgrid application requires control methods that achieve high performance not only during normal operating conditions, but also under unbalanced conditions. These conditions can occur permanently due to distribution of unbalanced loads on the three phases of the microgrid. This paper proposes a robust control strategy for a grid-connected multi-bus microgrid containing several inverter-based DG units. Each of the DG units can supply a combination of balanced and unbalanced local loads. The proposed control strategy employs an adaptive Lyapunov function based control scheme to directly compensate the negative-sequence current components caused by unbalanced loads in some part of microgrid; and a sliding mode based control scheme to directly regulate the positive-sequence active and reactive power injected by DG units to the microgrid. The control method proposed in this paper is shown to be robust and stable under load disturbances and microgrid parameter uncertainties even in the presence of nonlinear and time-variant unbalanced loads. The effectiveness of the presented controller is validated through time-domain simulation studies, under the MATLAB/Simulink software environment.

Introduction

Recently, due to a general increasing demand for electrical energy and a rising interest in clean technologies, the energy sector is moving to the era of distributed energy resources (DERs), such as wind turbines, photovoltaic systems, fuel-cells, micro-turbines and hydropower turbines [1,2]. Typical modern distributed generation (DG) units, which are collectively referred to DERs, do not generate 50/60 Hz ac voltages and therefore require electronic power converters as the interfacing medium between a prime energy source and the network [3–5].

The application of individual DG system has some major issues such as limited capacity and high cost per watts [4]. To solve the common problems of individual DG units in power systems, researchers have introduced a new concept called microgrid [6]. Microgrid is usually a part of distribution subsystem, which consists of cluster of loads and multiple DG units. A microgrid can be operated either in grid-connected mode or in islanding mode. Normally, microgrids operate in grid-connected mode because main-grid can support the system frequency and bus voltages by covering the power mismatch immediately. In the grid-connected operation, the microgrid is connected to main-grid at the point of common coupling (PCC), and each DG unit generates proper real and reactive power [7,8]. The PCC voltage is dominantly determined by main-grid, and the main role of the microgrid is to accommodate the load demand and the real or reactive power generated by the DG-units [9,10]. Proper operation of the microgrid requires high performance control techniques, not only during normal operating conditions, but also under unbalanced conditions [11].

Besides the primary purpose of the DG units, compensation of power quality problems can also be achieved through proper control strategies [12]. Among various power quality phenomena, voltage unbalances are very common. A major cause of voltage unbalance in a microgrid is the connection of unbalanced loads. In the conventional distribution systems, most of the unbalanced loads can compensate each other because many loads are installed [13]. Nevertheless, in the microgrid systems, unbalanced loads are very common and result from the uneven distribution of numerable loads among the three phases [14]. Therefore, a microgrid should be controlled in such a way that can operate under unbalanced load conditions without any performance degradations [15].

Unbalanced loads can cause the lines current and hence the microgrid voltage suffering from significant values of negative-sequence which can lead to increased losses, abnormal second

* Corresponding author at: Department of Technical & Engineering, Science and Research Branch, Islamic Azad University, Tehran, Iran.
E-mail address: mm.rezaei@srbiau.ac.ir (M.M. Rezaei).
[1] Emeritus professor of the Faculty of Electrical and Computer Engineering, Isfahan University of Technology.

http://dx.doi.org/10.1016/j.ijepes.2015.02.041
0142-0615/

Nomenclature

Variables

$\mathbf{v}_i, \mathbf{v}_f, \mathbf{v}_c$	inverter, filter, PCC voltage vectors
$\mathbf{i}_f, \mathbf{i}_L, \mathbf{i}_l$	filter, local load, line current vectors
$v_{\alpha\beta}, i_{\alpha\beta}$	$\alpha\beta$ components of voltage and current
V, I	voltage and current amplitude
R, L, C	resistance, inductance, capacitance
P, Q	active and reactive powers
S	sliding surface
e	tracking error
W	Lyapunov function

Superscripts

p, n	positive-, negative-sequence components
2ω	double-frequency oscillating component
ref	reference value

harmonic at the dc-link, and negative effects on equipment such as induction motors, power electronic converters, and adjustable speed drives [16,17]. Note that unbalanced loads are often connected on the wye side of a delta to grounded-wye transformer. Therefore the zero-sequence current is isolated from the delta side [9].

Several methods have been proposed in the literature for compensation of microgrid unbalances [16–22]. A vector control approach for controlling the voltage source converter (VSC) which is capable of mitigating the harmonics under unbalanced operating conditions is proposed in [18]. The method in [18] is implemented in stator-voltage-orientation synchronous reference frame, based on proportional-integral (PI) controllers. However, the main drawbacks for this control method are the tuning of the controller parameters, the necessity of synchronous coordinate transformations, the tracking of grid voltage phase angle, and the complexity of method. Moreover, the proposed control method is highly sensitive to variations of system parameters, but no parametric uncertainty is considered [23–25].

A direct power control strategy has been presented in [19,20] for a grid-connected VSC under voltage unbalanced conditions. The power control scheme is based on the sliding mode control approach, which controls the instantaneous active and reactive powers in the stationary reference frame. Three power control targets have been proposed during network unbalance to obtaining sinusoidal and symmetrical grid current, removing reactive power ripples, and canceling active power ripples. However in the chosen study system, the VSC is directly connected to main-grid that makes the system control very simple. In addition, the effectiveness and validity of proposed methods in the presence of loads has not been demonstrated. Furthermore, the NS power control method has been designed based on knowledge of actual values of the resistances and inductances of the system. Hence, the system stability is not guaranteed with subject to system parametric uncertainties.

A combination of the deadbeat and repetitive control has been used in [21] to compensate the impact of load imbalance on the performance of a single-bus microgrid. The control method of [21] is based on the vector control approach described in [18], and implemented in the discrete-time domain. However, the presented control method is complex and its effectiveness is not investigated in the multi-bus microgrids.

The control method described in [22] uses a linear proportional-resonant-based controller in combination with a PI-based virtual impedance controller in order to regulate the load voltage and compensate the negative-sequence (NS) current of unbalanced loads. In [22], two separated and independent equivalent circuits have been used for load positive-sequence (PS) and NS current components. One may note that in a three-phase circuit with unbalanced loads, the PS and NS components of load voltage are linear functions of both the PS and NS components of load current. It means that the equivalent circuits, used in [22], are not independent and should be electrically coupled. In addition, the stability and robustness of proposed control system, with respect to microgrid parametric uncertainties, is not verified.

The main contribution of this paper is to design a control structure, based on well-known LF and SM control techniques, in order to (1) compensate the negative-sequence current components caused by unbalanced loads in some part of a grid-connected multi-bus microgrid containing several inverter-based DG units and a combination of balanced and unbalanced loads; and (2) regulate the positive-sequence active and reactive power injected by DG units to the microgrid under both balanced and unbalanced conditions. In the designed controller, the load dynamics are masked and the DG unit dynamic performances are made independent of load characteristics and circuit configuration. Moreover, to overcome the computational burden associated with the tracking of grid voltage phase angle and frame transformations, the proposed controller is performed in stationary reference frame. The control method proposed in this paper is shown to be robust and stable under load disturbances and microgrid parameters uncertainties even in the presence of nonlinear loads. Some simulation results are presented to support the validity and effectiveness of the proposed control method.

Microgrid structure description

Fig. 1(a) shows a single-line diagram of the microgrid study system. The microgrid includes two inverter-based DG units and a cluster of loads. Each DG unit is connected to the corresponding point of connection (PC) through a LC filter to reduce the voltage ripple (and hence, the current ripple) caused by the switching. The local load of each DG unit is connected to the corresponding PC and is a combination of balanced and unbalanced loads. The common load is connected to the PCC and is a balanced load. The interlink-line 1 and 2 (hereafter, line 1 and 2), which connect PCs to the PCC, are represented by series RL branches. In this paper, it is assumed that the microgrid is connected to main-grid. The microgrid parameters are given in Table 1.

Modeling of a three-phase DG unit

Fig. 1(b) shows the control scheme of an inverter-based DG unit with LC-filter microgrid-interface. By using the well-known Clarke transformation, the current and voltage dynamics in the stationary ($\alpha\beta$) reference frame can be derived as:

$$\frac{d\mathbf{i}_f}{dt} = \frac{1}{L_f}(\mathbf{v}_\mathbf{i} - R_f\mathbf{i}_f - \mathbf{v}_f) \tag{1}$$

$$\frac{d\mathbf{v}_f}{dt} = \frac{1}{C_f}(\mathbf{i}_f - \mathbf{i}_L - \mathbf{i}_l) \tag{2}$$

$$\frac{d\mathbf{i}_l}{dt} = \frac{1}{L_l}(\mathbf{v}_f - R_l\mathbf{i}_l - \mathbf{v}_c) \tag{3}$$

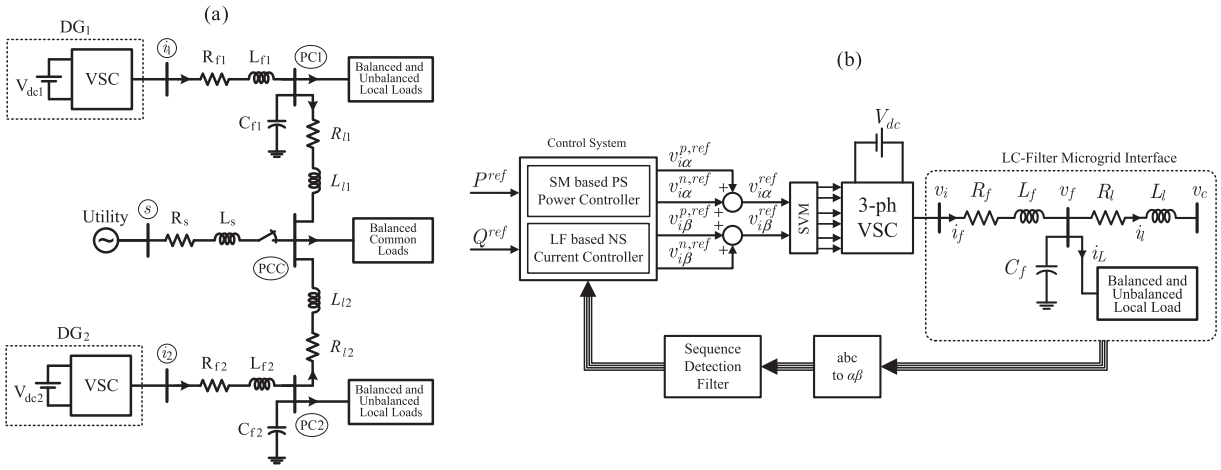

Fig. 1. (a) Schematic diagram of the microgrid under consideration; (b) proposed control scheme.

Table 1
System parameters.

Grid voltage, Line to Line, rms	v_s	380 V
Fundamental frequency	f_s	50 Hz
Grid resistance	R_s	0.020 Ω
Grid inductance	L_s	200 μH
Line1 resistance	R_{l1}	0.050 Ω
Line1 inductance	L_{l1}	100 μH
Line2 resistance	R_{l2}	0.060 Ω
Line2 inductance	L_{l2}	120 μH
dc bus voltage	V_{dc}	800 V
Filter resistance	R_{f1}, R_{f2}	0.050 Ω
Filter inductance	L_{f1}, L_{f2}	800 μH
Filter capacitance	C_{f1}, C_{f2}	200 μF
Switching frequency	f_{sw}	6480 Hz

It is assumed that the LC-filters and the lines have balanced three-phase impedances and as a result, the equations (1)–(3) can be fully decoupled into positive and negative sequences. Under unbalanced condition, each of voltages and currents can be expressed as [26]:

$$\mathbf{v} = [\, v_\alpha \quad v_\beta \,]^T = [\, (v_\alpha^p + v_\alpha^n) \quad (v_\beta^p + v_\beta^n) \,]^T \tag{4}$$

$$\mathbf{i} = [\, i_\alpha \quad i_\beta \,]^T = [\, (i_\alpha^p + i_\alpha^n) \quad (i_\beta^p + i_\beta^n) \,]^T \tag{5}$$

Since the whole controller is designed in the stationary reference frame, the sequence detection of microgrid voltages and currents is also realized based on a stationary frame notch filter in the $\alpha\beta$-frame [27]. As stated in [27], the applied method can tolerate a certain range of grid frequency variations. Although according to the allowable limits of frequency-deviation of main-grid [28], a phase-locked loop (PLL) can be avoided in the grid-connected mode [23,27], for adapting to wider range of grid frequency variations, a PLL or a frequency adaption loop should be added to the applied filter [27,29]. Thus, the proposed method can be easily adapted to fulfill the actual requirements for tolerating frequency variations in a microgrid context, although operation with frequency variation is not the focus of this paper.

Control design

The proposed control structure consists of a SM based PS power controller and an LF based NS current controller, as shown in Fig. 1(b). The power controller is designed to regulate the PS active and reactive power injected by DG unit to the microgrid. The current controller is designed to compensate the impact of NS current of the unbalanced loads. In the following subsections, the control design procedure is explained in detail.

SM Based PS power control

The instantaneous active and reactive power injected by DG unit to the PC bus can be represented as [24]:

$$P = \frac{3}{2}(\mathbf{v}_f \cdot \mathbf{i}_f) = \frac{3}{2}(v_{f\alpha} i_{f\alpha} + v_{f\beta} i_{f\beta}) \tag{6}$$

$$Q = -\frac{3}{2}|\mathbf{v}_f \times \mathbf{i}_f| = \frac{3}{2}(v_{f\beta} i_{f\alpha} - v_{f\alpha} i_{f\beta}) \tag{7}$$

where "·" denotes the inner-product and " × " represents the cross-product of two vectors and bold symbols *represent* $\mathbf{v}_f = [\, v_{f\alpha}\ v_{f\beta} \,]^T$ and $\mathbf{i}_f = [\, i_{f\alpha}\ i_{f\beta} \,]^T$. Under unbalanced conditions, the instantaneous active and reactive powers can be expressed by the PS and NS components of the voltages and currents as given by (8) and (9), respectively [24].

$$P = P^p + P^n + P^{2\omega} \tag{8}$$

$$Q = Q^p + Q^n + Q^{2\omega} \tag{9}$$

with:

$$\begin{bmatrix} P^p \\ Q^p \end{bmatrix} = \frac{3}{2} \begin{bmatrix} v_{f\alpha}^p & v_{f\beta}^p \\ v_{f\beta}^p & -v_{f\alpha}^p \end{bmatrix} \begin{bmatrix} i_{f\alpha}^p \\ i_{f\beta}^p \end{bmatrix} \tag{10}$$

$$\begin{bmatrix} P^n \\ Q^n \end{bmatrix} = \frac{3}{2} \begin{bmatrix} v_{f\alpha}^n & v_{f\beta}^n \\ v_{f\beta}^n & -v_{f\alpha}^n \end{bmatrix} \begin{bmatrix} i_{f\alpha}^n \\ i_{f\beta}^n \end{bmatrix} \tag{11}$$

$$\begin{bmatrix} P^{2\omega} \\ Q^{2\omega} \end{bmatrix} = \frac{3}{2} \begin{bmatrix} v_{f\alpha}^p & v_{f\beta}^p \\ v_{f\beta}^p & -v_{f\alpha}^p \end{bmatrix} \begin{bmatrix} i_{f\alpha}^n \\ i_{f\beta}^n \end{bmatrix} + \frac{3}{2} \begin{bmatrix} v_{f\alpha}^n & v_{f\beta}^n \\ v_{f\beta}^n & -v_{f\alpha}^n \end{bmatrix} \begin{bmatrix} i_{f\alpha}^p \\ i_{f\beta}^p \end{bmatrix} \tag{12}$$

where $P^{2\omega}$ and $Q^{2\omega}$ denote the double frequency oscillating components of the respective active and reactive power, which generated from the interaction between PS voltage and NS current and/or NS voltage and PS current, as expressed by (12) [24]. Noting that under balanced conditions, the NS components of voltages and currents are zero and thus, the instantaneous powers are equal to PS power components. It means that under both balanced and unbalanced load conditions, the PS active and reactive powers should be controlled. In the proposed control strategy, the regulation of PS active and reactive power components has been implemented by using

sliding mode control method due to its fast-tracking capability and its robustness against disturbances, parametric uncertainties and modeling approximations [30]. In the present control design problem, the following integral-based sliding surface is chosen to obtain active and reactive power regulation.

$$\begin{bmatrix} S_P \\ S_Q \end{bmatrix} = \begin{bmatrix} e_P \\ e_Q \end{bmatrix} + k_s \int_0^t \begin{bmatrix} e_P \\ e_Q \end{bmatrix} d\tau \tag{13}$$

where $e_P = P^{ref} - P^p$ and $e_Q = Q^{ref} - Q^p$ are the active and reactive power tracking errors, and $k_s = diag[k_{sP}, k_{sQ}]$ is a diagonal matrix with all positive constant diagonal entries which are the SM control gains. Based on SM control theory, it is required to restrict the controlled states onto its corresponding sliding surfaces [30]. This is exclusively governed by:

$$S = \frac{dS}{dt} = 0 \tag{14}$$

Considering (14), differentiating (13) with respect to time gives:

$$\frac{d}{dt}\begin{bmatrix} S_P \\ S_Q \end{bmatrix} = \frac{d}{dt}\begin{bmatrix} P^{ref} - P^p \\ Q^{ref} - Q^p \end{bmatrix} + k_s \begin{bmatrix} e_P \\ e_Q \end{bmatrix} = -\frac{d}{dt}\begin{bmatrix} P^p \\ Q^p \end{bmatrix} + k_s \begin{bmatrix} e_P \\ e_Q \end{bmatrix} \tag{15}$$

By considering (10), it can be obtained that

$$\begin{bmatrix} \frac{dP^p}{dt} \\ \frac{dQ^p}{dt} \end{bmatrix} = \frac{3}{2}\begin{bmatrix} \frac{dv^p_{f\alpha}}{dt} & \frac{dv^p_{f\beta}}{dt} \\ \frac{dv^p_{f\beta}}{dt} & -\frac{dv^p_{f\alpha}}{dt} \end{bmatrix}\begin{bmatrix} i^p_{f\alpha} \\ i^p_{f\beta} \end{bmatrix} + \frac{3}{2}\begin{bmatrix} v^p_{f\alpha} & v^p_{f\beta} \\ v^p_{f\beta} & -v^p_{f\alpha} \end{bmatrix}\begin{bmatrix} \frac{di^p_{f\alpha}}{dt} \\ \frac{di^p_{f\beta}}{dt} \end{bmatrix} \tag{16}$$

Substituting for $\frac{d}{dt} v^p_{f\alpha\beta}$ and $\frac{d}{dt} i^p_{f\alpha\beta}$, respectively from (2) and (1), into (16), results in:

$$\begin{aligned} \begin{bmatrix} \frac{dP^p}{dt} \\ \frac{dQ^p}{dt} \end{bmatrix} = {} & \frac{3}{2C_f}\begin{bmatrix} (i^p_{f\alpha} - i^p_{L\alpha} - i^p_{l\alpha}) & (i^p_{f\beta} - i^p_{L\beta} - i^p_{l\beta}) \\ (i^p_{f\beta} - i^p_{L\beta} - i^p_{l\beta}) & -(i^p_{f\alpha} - i^p_{L\alpha} - i^p_{l\alpha}) \end{bmatrix}\begin{bmatrix} i^p_{f\alpha} \\ i^p_{f\beta} \end{bmatrix} \\ & + \frac{3}{2L_f}\begin{bmatrix} v^p_{f\alpha} & v^p_{f\beta} \\ v^p_{f\beta} & -v^p_{f\alpha} \end{bmatrix}\begin{bmatrix} (v^p_{i\alpha} - v^p_{f\alpha} - R_f i^p_{f\alpha}) \\ (v^p_{i\beta} - v^p_{f\beta} - R_f i^p_{f\beta}) \end{bmatrix} \end{aligned} \tag{17}$$

By substituting for $\frac{d}{dt} P^p$ and $\frac{d}{dt} Q^p$ from (17) into (15), it can be shown that:

$$\frac{d}{dt}\begin{bmatrix} S_P \\ S_Q \end{bmatrix} = -\begin{bmatrix} G_P \\ G_Q \end{bmatrix} - \begin{bmatrix} H_P \\ H_Q \end{bmatrix} - \frac{3}{2L_f}\begin{bmatrix} v^p_{f\alpha} & v^p_{f\beta} \\ v^p_{f\beta} & -v^p_{f\alpha} \end{bmatrix}\begin{bmatrix} v^p_{i\alpha} \\ v^p_{i\beta} \end{bmatrix} + k_s \begin{bmatrix} e_P \\ e_Q \end{bmatrix} \tag{18}$$

with:

$$\begin{aligned} G_P &= \frac{3}{2C_f}((i^p_{f\alpha} - i^p_{L\alpha} - i^p_{l\alpha})i^p_{f\alpha} + (i^p_{f\beta} - i^p_{L\beta} - i^p_{l\beta})i^p_{f\beta}) \\ G_Q &= \frac{3}{2C_f}((i^p_{f\beta} - i^p_{L\beta} - i^p_{l\beta})i^p_{f\alpha} - (i^p_{f\alpha} - i^p_{L\alpha} - i^p_{l\alpha})i^p_{f\beta}) \\ H_P &= -\frac{3}{2L_f}((v^p_{f\alpha} + R_f i^p_{f\alpha})v^p_{f\alpha} + (v^p_{f\beta} + R_f i^p_{f\beta})v^p_{f\beta}) \\ H_Q &= -\frac{3}{2L_f}((v^p_{f\alpha} + R_f i^p_{f\alpha})v^p_{f\beta} - (v^p_{f\beta} + R_f i^p_{f\beta})v^p_{f\alpha}) \end{aligned} \tag{19}$$

By considering (14), the SM control effort $\begin{bmatrix} v^p_{i\alpha} & v^p_{i\beta} \end{bmatrix}^T$ can be obtained by solving the following equation:

$$\frac{d}{dt}\begin{bmatrix} S_P \\ S_Q \end{bmatrix} = 0 \tag{20}$$

By combining (18) and (20), the control law can be obtained as:

$$\begin{bmatrix} v^{p,ref}_{i\alpha} \\ v^{p,ref}_{i\beta} \end{bmatrix} = \frac{2L_f}{3}\begin{bmatrix} v^p_{f\alpha} & v^p_{f\beta} \\ v^p_{f\beta} & -v^p_{f\alpha} \end{bmatrix}^{-1}\left\{-\begin{bmatrix} G_P \\ G_Q \end{bmatrix} - \begin{bmatrix} H_P \\ H_Q \end{bmatrix} + k_s \begin{bmatrix} e_P \\ e_Q \end{bmatrix}\right\} \tag{21}$$

with:

$$\begin{bmatrix} v^p_{f\alpha} & v^p_{f\beta} \\ v^p_{f\beta} & -v^p_{f\alpha} \end{bmatrix}^{-1} = \frac{-1}{(v^p_{f\alpha})^2 + (v^p_{f\beta})^2}\begin{bmatrix} -v^p_{f\alpha} & -v^p_{f\beta} \\ -v^p_{f\beta} & v^p_{f\alpha} \end{bmatrix} = \frac{1}{(V^p_f)^2}\begin{bmatrix} v^p_{f\alpha} & v^p_{f\beta} \\ v^p_{f\beta} & -v^p_{f\alpha} \end{bmatrix} \tag{22}$$

According to SM control theory, the process of SM control can be divided into two phases, that is, the reaching phase and the sliding phase [30]. The control law given by (21) is only valid for sliding phase of the SM control process. The control effort which guarantees the SM control in both the reaching and sliding phases can be represented by [30]:

$$\begin{aligned} \begin{bmatrix} v^{p,ref}_{i\alpha} \\ v^{p,ref}_{i\beta} \end{bmatrix} = {} & \frac{2L_f}{3(V^p_f)^2}\begin{bmatrix} v^p_{f\alpha} & v^p_{f\beta} \\ v^p_{f\beta} & -v^p_{f\alpha} \end{bmatrix}\left\{-\begin{bmatrix} G_P \\ G_Q \end{bmatrix} - \begin{bmatrix} H_P \\ H_Q \end{bmatrix} + k_s \begin{bmatrix} e_P \\ e_Q \end{bmatrix}\right. \\ & \left. + k_v \begin{bmatrix} \mathrm{sgn}(S_P) \\ \mathrm{sgn}(S_Q) \end{bmatrix}\right\} \end{aligned} \tag{23}$$

where $k_v = \mathrm{diag}[k_{vP}, k_{vQ}]$ is a diagonal matrix with all positive constant diagonal entries which are the SM control gains and, the sign function sgn(·) is described by:

$$\mathrm{sgn}(x) = |x|/x \tag{24}$$

Based on Lyapunov's direct method of stability [30], the overall stability of the control system has been shown in the paper Appendix A. It can be seen from (23) that the operation of the proposed power controller is directly affected by positive sequence PC voltage amplitude. When the PC voltage drops, the power controller, in response to the drop, increases the current of the DG converter. To prevent an excessive output current, the active and reactive power references should be limited as a function of the actual grid voltage amplitude. Based on the maximum limit of converter output current $I_{\max}$, and the active and reactive power references, the minimum amplitude of the PC voltage $V_{\min}$, which corresponds to the maximum output current, can be obtained as:

$$V_{\min} = \frac{\sqrt{(P^{ref})^2 + (Q^{ref})^2}}{I_{\max}} \tag{25}$$

If $V^p_f < V_{\min}$, the active and reactive power delivered by the DG unit should be limited to:

$$\begin{cases} P_{\max} = I_{\max} V_f \cos(\varphi) \\ Q_{\max} = I_{\max} V_f \sin(\varphi) \end{cases} \tag{26}$$

with:

$$\varphi = \tan^{-1}\left(\frac{Q^{ref}}{P^{ref}}\right) \tag{27}$$

Based on (26), a dynamic limiter can be designed for P^{ref} and Q^{ref} to ensure that converter output current is within the allowable limits. Therefore, the over-current protection of converter can be easily ensured in case of grid voltage drops, although this is not the main focus of this paper.

NS current control based on LF

Referring to Fig. 1(b), a combination of balanced and unbalanced loads is assumed to be connected to each PC bus. To compensate the NS currents of the unbalanced loads, two comparable control objectives are presented in this paper. The first is to obtain symmetrical and sinusoidal DG output current that lead to compensate the NS currents of unbalanced loads by main-grid. In this case, the NS components of DG output current should be removed. The second is to obtain symmetrical and sinusoidal line current that lead to supply the NS currents of each unbalanced load by

the corresponding DG unit. So, the system outputs are NS components of DG output current $\boldsymbol{i}_f^n = \begin{bmatrix} i_{f\alpha}^n & i_{f\beta}^n \end{bmatrix}^T$. Our purpose is to make the output $\boldsymbol{i}_f^n$ track the desired trajectory, that under first control objective is zero, and under second control objective is:

$$\boldsymbol{i}_f^{n,ref} = \begin{bmatrix} i_{f\alpha}^{n,ref} \\ i_{f\beta}^{n,ref} \end{bmatrix} = \begin{bmatrix} i_{L\alpha}^{n} \\ i_{L\beta}^{n} \end{bmatrix} \tag{28}$$

In the proposed control structure, the NS current controller has been implemented by using adaptive Lyapunov function method. This method can achieve the goals of stabilization, tracking and parameter estimation [30,31]. The design procedure of the mentioned current controller is explained as follows. Considering the parameters in the nominal condition, equation (1) can be rewritten as:

$$\frac{d\boldsymbol{i}_f^n}{dt} = a(\mathbf{v}_i^n - b\boldsymbol{i}_f^n - \mathbf{v}_f^n) \tag{29}$$

where $a = \frac{1}{L_f}$ and $b = R_f$ are the nominal parameter values. If the parameters of the system deviate from their nominal values, the dynamic equation (29) can be modified as:

$$\frac{d\boldsymbol{i}_f^n}{dt} = a(\mathbf{v}_i^n - b\boldsymbol{i}_f^n - \mathbf{v}_f^n) + \boldsymbol{\xi} \tag{30}$$

where $\boldsymbol{\xi} = \begin{bmatrix} \xi_\alpha & \xi_\beta \end{bmatrix}^T$ is the lumped-sum uncertainty which can be written as:

$$\boldsymbol{\xi} = \Delta a(\mathbf{v}_i^n - b\boldsymbol{i}_f^n - \mathbf{v}_f^n) + \Delta b(a + \Delta a)\boldsymbol{i}_f^n \tag{31}$$

where "Δ" denotes deviation from nominal value. Letting

$$e_1 = \boldsymbol{i}_f^{n,ref} - \boldsymbol{i}_f^n \tag{32}$$

be the tracking error, and

$$e_\xi = \hat{\boldsymbol{\xi}} - \boldsymbol{\xi} \tag{33}$$

be the error between lump-sum uncertainties ξ and its estimated value $\hat{\boldsymbol{\xi}} = \begin{bmatrix} \hat{\xi}_\alpha & \hat{\xi}_\beta \end{bmatrix}^T$, a Lyapunov function can be defined as follows [31]:

$$W_1 = \frac{1}{2}e_1^T e_1 + \frac{1}{2}e_\xi^T \boldsymbol{\gamma} e_\xi \tag{34}$$

where $\boldsymbol{\gamma} = \mathrm{diag}[\gamma_\alpha, \gamma_\beta]$ is a diagonal matrix with all positive constant diagonal entries which are the adaptation law gains.

Differentiating W_1 with respect to time gives:

$$\frac{d}{dt}W_1 = e_1^T \frac{d}{dt}e_1 + e_\xi^T \boldsymbol{\gamma} \frac{d}{dt}e_\xi \tag{35}$$

Considering (30), (32) and (33), it can be shown that:

$$\frac{d}{dt}W_1 = e_1^T\left(\frac{d}{dt}\boldsymbol{i}_f^{n,ref} - a(\mathbf{v}_i^n - b\boldsymbol{i}_f^n - \mathbf{v}_f^n) - \boldsymbol{\xi}\right) + e_\xi^T \boldsymbol{\gamma}\left(\frac{d}{dt}\hat{\boldsymbol{\xi}}\right) \tag{36}$$

If the adaptation law is chosen as:

$$\frac{d}{dt}\hat{\boldsymbol{\xi}} = -\boldsymbol{\gamma}^{-1}e_1 \tag{37}$$

then $\frac{d}{dt}W_1$ becomes

$$\frac{d}{dt}W_1 = e_1^T\left(\frac{d}{dt}\boldsymbol{i}_f^{n,ref} - a(\mathbf{v}_i^n - b\boldsymbol{i}_f^n - \mathbf{v}_f^n) - \hat{\boldsymbol{\xi}}\right). \tag{38}$$

To stabilize e_1, $\frac{d}{dt}W_1$ should be negative definite. Now, if the control input $\mathbf{v}_i^n$ is selected as:

$$\mathbf{v}_i^n = b\boldsymbol{i}_f^n + \mathbf{v}_f^n + \frac{1}{a}\left(\frac{d}{dt}\boldsymbol{i}_f^{n,ref} - \hat{\boldsymbol{\xi}} + k_1 e_1\right) \tag{39}$$

where $k_1 = diag[k_{1\alpha}, k_{1\beta}]$ is a positive constant diagonal matrix, then, $\frac{d}{dt}W_1$ can be given by:

$$\frac{d}{dt}W_1 = -\boldsymbol{k}_1 e_1^T e_1 \tag{40}$$

Since the time-derivative of Lyapunov function W_1 is definitely negative, the proposed current control system is asymptotically stable.

Implementation of the proposed control scheme

As shown in Fig. 1(b), the positive- and negative-sequence components of the control signals, generated by PS power controller and NS current controller, are finally summed up to generate the converter voltage references, as an input to space vector modulation (SVM) module. It should be noted that, in order to avoid unexpected chattering near the sliding surface, the sign function in PS and NS control efforts expressed in (23) is changed into a saturation function, which is described by:

$$\mathrm{sat}(x) = \begin{cases} \mathrm{sgn}(x) & |x| > \lambda \\ x/\lambda & |x| \leqslant \lambda \end{cases} \tag{41}$$

where λ is a positive constant.

Simulation results

In order to evaluate the effectiveness of the presented control strategy, the microgrid study system shown in Fig. 1(a) has been simulated in the MATLAB/Simulink software environment. All DG units are equipped with the proposed controller. Several detailed load switching are carried out to demonstrate the steady-state and dynamic performances of the proposed control strategy. In the simulation studies, while the system is initially operating under balanced condition, an unbalanced load is connected to PC1 at $t = 2$ s. The unbalanced load consists of a series RL circuit between phase-b and phase-c; the load resistance and inductance are 25 Ω and 60 mH.

The impact of nonlinear and time-variant unbalanced loads on the performance of proposed controller is investigated by applying a 4-pole, $\frac{1}{4}$ hp, 110 V and 50 Hz single-phase induction motor [32]. The motor is connected to PC2, between phase-b and phase-c, via a 380/110 V single-phase transformer. The used motor is a capacitor-start-capacitor-run single-phase induction motor with parameters given in the paper Appendix B. The motor is energized from $t = 3$ s and the start-capacitor is tripped when the motor is speeded up to 75% of the rated speed. Subsequently, at $t = 4$ s, the balanced load of PC1 is disconnected and later at $t = 5$ s, the single-phase motor is switched off. Moreover, to evaluate the robust performance of proposed controller subject to parametric uncertainties, a 20% step-mismatch is assumed for filter resistances from $t = 2.5$ s.

In the simulation studies, both the proposed control objectives including (1) PS power regulation and NS current elimination of the DG unit; and (2) PS power regulation of the DG unit and NS current elimination of the interlink-line; are evaluated. The power reference values are given in the paper Appendix B. Some simulation results obtained for this case study are shown in Figs. 2-10. In the graphs, the real powers, reactive powers, voltages and currents are expressed in kilowatts, kilo-volt-amperes-reactive, volts and amperes, respectively.

Figs. 2 and 3 show the amplitude of detected NS current of local loads, DG units and lines, respectively, under first and second control objectives. All these quantities are calculated by:

$$I = \sqrt{(i_\alpha)^2 + (i_\beta)^2} \tag{42}$$

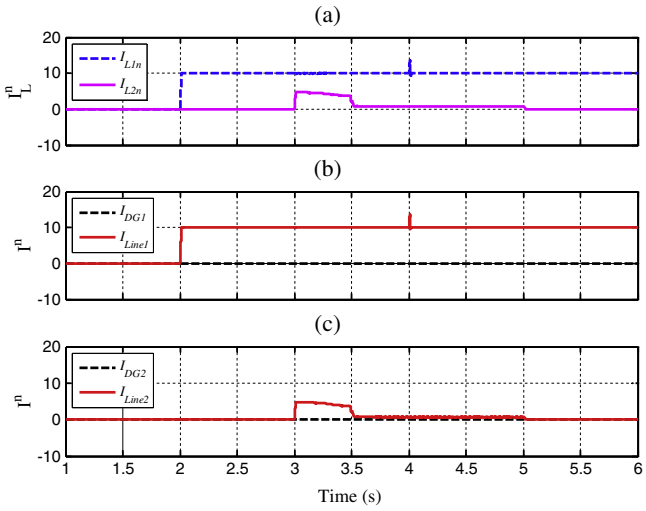

Fig. 2. Amplitude of (a) NS current of local loads, (b) NS current of DG1 and line1, and (c) NS current of DG2 and line2, all under first control objective.

As indicated in Figs. 2(a) and 3(a), since the load of PC1 and PC2 become unbalanced, the NS component of loads currents is increased. As shown in Fig. 2(b) and (c), under first control objective, the NS currents of DG units are removed, while the NS currents of local loads are supplied by main-grid, which flow in the lines. Under second control objective, the NS components of converter reference voltages are adaptively changed to supply the NS current components of local loads. Therefore, the NS component of the lines current is removed, as indicated in Fig. 3(b) and (c). Figs. 2 and 3 show that despite the mismatched filter resistances and the time-varying disturbance due to the motor startup, both the proposed NS current control schemes exhibit a desirable performance.

Figs. 4 and 5 illustrate a zoomed view of NS current amplitude of DG1 and line1, and the waveforms of v_{f1-abc}, i_{f1-abc} and i_{l1-abc} prior and subsequent to the connection of the unbalanced load of PC1 at $t = 2$ s, respectively, under first and second control objectives. It can be seen that under first control objective (Fig. 4), the DG current is not imposed by unbalanced load current and remained balanced and transient-free. Under these conditions the load current imbalance is compensated by main-grid. Fig. 5 shows that under second control objective, the load current imbalance is

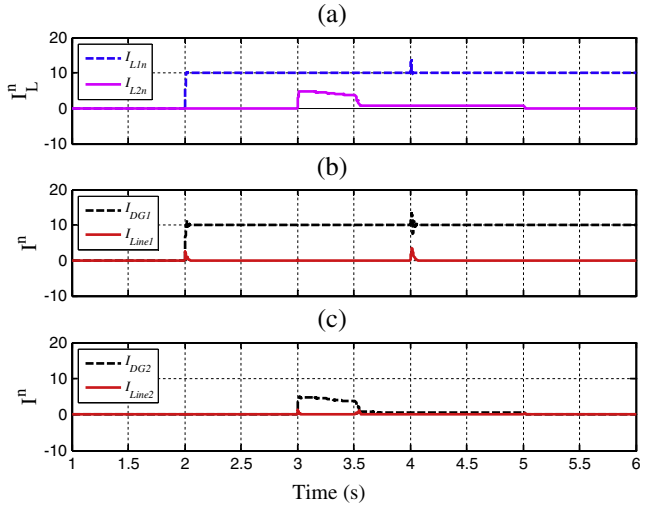

Fig. 3. Amplitude of (a) NS current of local loads, (b) NS current of DG1 and line1, and (c) NS current of DG2 and line2, all under second control objective.

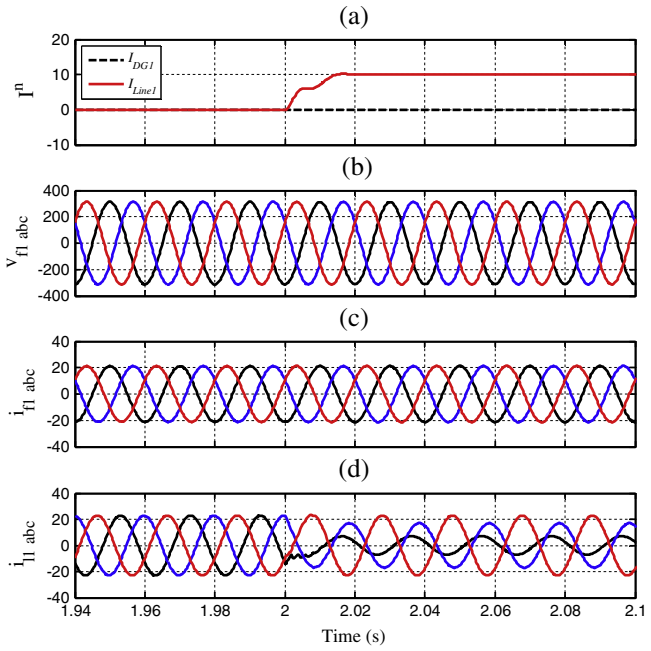

Fig. 4. Zoomed view of the waveforms of (a) NS current amplitude of DG1 and line1; (b) v_{f1-abc}; (c) i_{f1-abc}; and (c) i_{l1-abc} under first control objective.

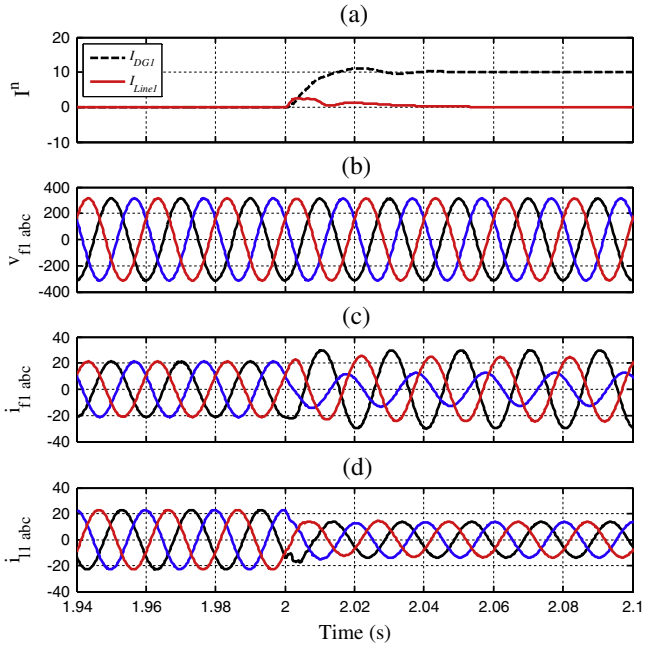

Fig. 5. Zoomed view of the waveforms of (a) NS current amplitude of DG1 and line1; (b) v_{f1-abc}; (c) i_{f1-abc}; and (c) i_{l1-abc} under second control objective.

compensated by DG unit and the line current reaches its sinusoidal and symmetrical steady-state with a reasonable transient performance.

Fig. 6 indicates the voltage-unbalance-factor (VUF) of PCC voltage (i.e. the ratio of the NS to PS components of the PCC voltage). Under first control objective, the NS components of load currents are compensated by main grid. Therefore, the unbalanced loads can cause the line currents suffering from high values of negative-sequence which can lead to microgrid voltage imbalance (Fig. 6(a)). Under second control objective (Fig. 6(b)), the NS components of load currents are supplied by DG units. Therefore, the

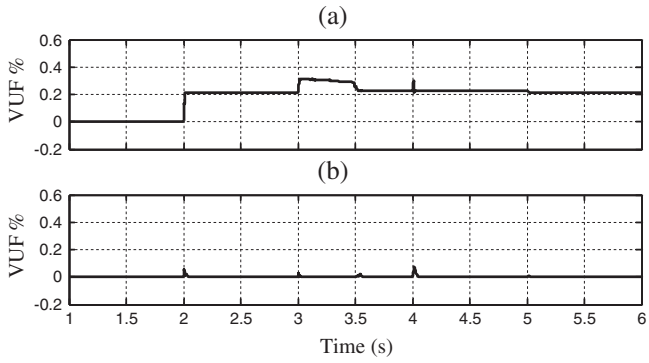

Fig. 6. Voltage-unbalance-factor of PCC, (a) under first and (b) under second control objective.

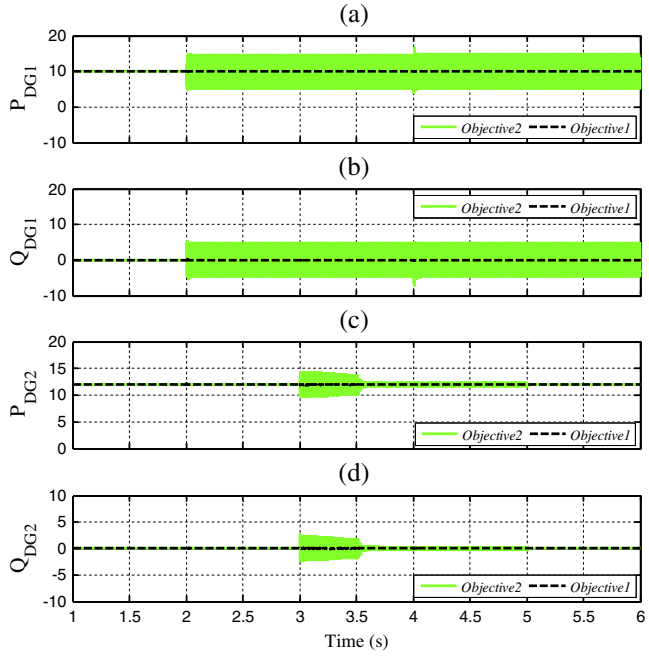

Fig. 7. Instantaneous active and reactive power of DG units, under both control objectives.

line currents and busbar voltages are not affected by unbalanced loads and remained balanced.

Fig. 7 shows the instantaneous active and reactive power of DG units, under both the first and second control objective. Considering these plots, it can be seen that the average values of active and reactive power of DG units very well track their corresponding references, even under load switching and unbalanced load conditions. However, under the second control objective, the instantaneous active and reactive power components of DG units are imposed by double frequency oscillations (DFOs). The DFOs appeared in the power of each DG unit is proportional to its NS currents.

Fig. 8 shows the instantaneous active and reactive power of the lines, under both the first and second control objectives. The step changes seen in the average value of active and reactive powers are due to described step changing of loads demand. The DFOs seen in Fig. 9 are due to unbalanced lines currents under first control objective.

Fig. 9(a) and (b) provide a zoomed view of Figs. 7(a) and 8(a), respectively, over a period around $t = 2$ s subsequent to the energization of the unbalanced load of PC1. As shown, while the second

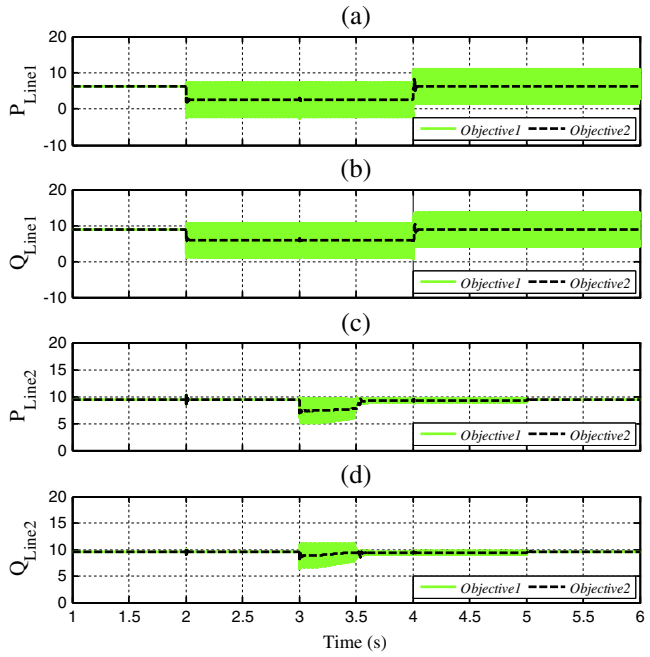

Fig. 8. Instantaneous active and reactive power of lines, under both control objectives.

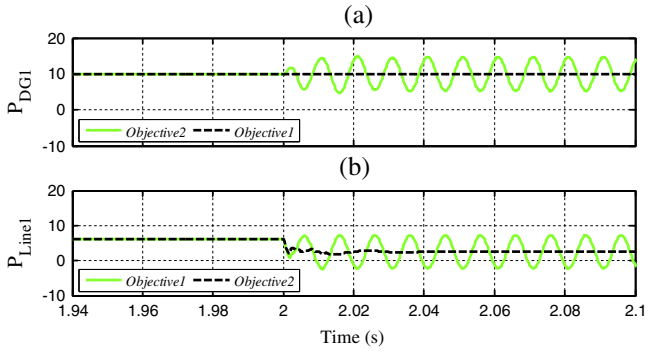

Fig. 9. Zoomed view of (a) P_{DG1} and (b) P_{Line1} under both control objective.

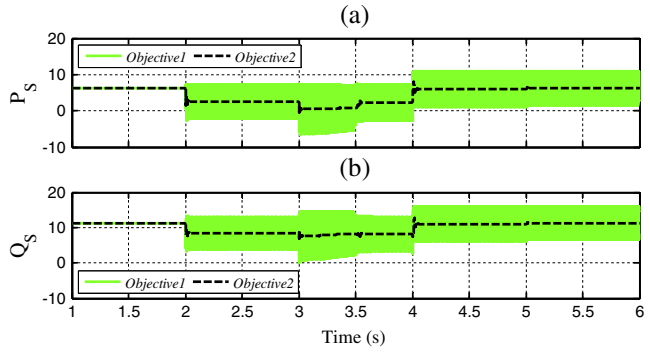

Fig. 10. Instantaneous active and reactive power injected to main grid under both control objective.

control objective has a reasonable transient response, the first control objective exhibits no observable transient since the NS current controllers rapidly track the zero references and remove the NS component of DGs output current.

Fig. 10 shows the instantaneous active and reactive power injected by microgrid to main-grid, under both the first and second control objectives. The DFOs seen in Fig. 10 are due to lines current imbalance, under first control objective. Under second control objective, the instantaneous active and reactive power absorbed by main-grid exhibit no observable DFO because the NS current of unbalanced loads has been compensated by DG units. It should be noted that under second control objective, although the NS current of unbalanced loads has been compensated independently from main-grid, in islanded mode of operation, in order to regulate the voltage and frequency of the microgrid about rated values and, at the same time, properly share the active and reactive power between DG units, a proper control strategy (such us centralized-control, master/slave, or droop-based control methods) should be employed which is out of scope of this paper and can be addressed in future works.

Conclusion

This paper presents a robust controller for a grid-connected multi-bus microgrid containing several inverter-based DG units and unbalanced loads. The proposed control structure has two control modules consisting of a sliding mode based PS power controller and an adaptive NS current controller based on Lyapunov function method. The power controller ensures that the PS active and reactive power, generated by each DG unit, track its respective reference commands under both balanced and unbalanced conditions. The current controller compensates the NS current of unbalanced local loads in some part of the microgrid. Two comparable control objectives are presented in this paper including: (1) PS power regulation and elimination of the NS components of DG current; and (2) PS power regulation and elimination of the line NS current components. The effectiveness of the proposed control structure is demonstrated through time-domain simulation studies, under the MATLAB/Simulink environment. Simulation results confirm that under second control objective, the NS current of lines is removed, the double frequency oscillations of the active and reactive power injected to main-grid are eliminated and, the power quality of the overall microgrid system is improved. However, under first control objective, the DGs current imbalance is significantly less than that obtained by second objective. Moreover, while the second control objective has a reasonable transient response, the first control objective exhibits no observable transients. Simulation results conclude that the proposed control strategy is robust and stable subject to load disturbances and microgrid parameters uncertainties even in the presence of nonlinear and time-variant unbalanced loads.

Appendix A

Consider the following positive definite Lyapunov function:

$$W_2 = \frac{1}{2}\begin{bmatrix} S_P & S_Q \end{bmatrix}\begin{bmatrix} S_P \\ S_Q \end{bmatrix} \tag{43}$$

Differentiating W_2 with respect to time gives:

$$\frac{d}{dt}W_2 = \begin{bmatrix} S_P & S_Q \end{bmatrix}\left(\frac{d}{dt}\begin{bmatrix} S_P \\ S_Q \end{bmatrix}\right) \tag{44}$$

Substituting (18) into (44) yields:

$$\frac{d}{dt}W_2 = \begin{bmatrix} S_P & S_Q \end{bmatrix}\left(-\begin{bmatrix} G_P \\ G_Q \end{bmatrix} - \begin{bmatrix} H_P \\ H_Q \end{bmatrix} - \frac{3}{2L_f}\begin{bmatrix} v^p_{f\alpha} & v^p_{f\beta} \\ v^p_{f\beta} & -v^p_{f\alpha} \end{bmatrix}\begin{bmatrix} v^p_{i\alpha} \\ v^p_{i\beta} \end{bmatrix} + k_s\begin{bmatrix} e_P \\ e_Q \end{bmatrix}\right) \tag{45}$$

By substituting (23) into (45), it can be obtained that:

$$\frac{d}{dt}W_2 = \begin{bmatrix} S_P & S_Q \end{bmatrix}\left(-k_v\begin{bmatrix} sgn(S_P) \\ sgn(S_Q) \end{bmatrix}\right) \tag{46}$$

The time-derivative of Lyapunov function $\frac{d}{dt}W_2$ is then definitely negative so that the power control system becomes asymptotically stable.

Appendix B

The power references and the parameters of the single-phase induction motor are given as follows: *Power references:* $P_{ref1} = 10kW$, $Q_{ref1} = 0kVAr$, $P_{ref2} = 12kW$, $Q_{ref2} = 0kVAr$; *Single-phase induction motor:* main winding stator resistance and inductance: 2.02 Ω and 7.4 mH, main winding rotor resistance and inductance: 4.12 Ω and 5.6 mH, main winding mutual inductance: 177.2 mH, auxiliary winding resistance and inductance: 7.14 Ω and 8.5 mH, capacitor start: 254.7 μF, capacitor run: 21.1 μF; *Balanced loads:* PCC-, PC1-, and PC2-connected balanced load's resistance and inductance: 10 Ω and 24 mH, 25 Ω and 60 mH, and 35 Ω and 90 mH, respectively.

References

[1] Shahidehpour M, Schwartz F. Don't let the sun go down on PV. IEEE Power Energ Mag 2004;2(3):40–8.
[2] IEEE Trans. Power Electron. Special issue on distributed power generation. IEEE, vol. 19(5), 2004. p. 1157–58.
[3] Mohamed YARI, El-Saadany EF, Salama MM. Adaptive grid-voltage sensorless control scheme for inverter-based distributed generation. IEEE Trans Energy Conv 2009;24(3):683–94.
[4] Zahraee MH, Bakhshai A. Transient Droop Control Strategy for Parallel Operation of Voltage Source Converters in an Islanded Mode Microgrid. In: Proc Int Telecommunications Energy Conf, 2011.
[5] Pogaku N, Prodanovic M, Green T. Modeling, analysis and testing of autonomous operation of an inverter-based microgrid. IEEE Trans Power Electron 2007;22(2):613–25.
[6] Hatziargyriou N, Asano H, Iravani MR, Marnay C. Microgrids. IEEE Power Energy Mag 2007;5(4):78–94.
[7] Li Y, Li YW. Power management of inverter interfaced autonomous microgrid based on virtual frequency-voltage frame. IEEE Trans Smart Grid 2011;2(1):30–40.
[8] Katiraei F, Iravani MR. Power management strategies for a microgrid with multiple distributed generation units. IEEE Trans Power Syst 2006;21(4):1821–31.
[9] Mehrizi-Sani A, Iravani MR. Potential-function based control of a microgrid in islanded and grid-connected modes. IEEE Trans Power Syst 2010;25(4):1883–91.
[10] Chung IY, Liu W, Cartes D, Collins E, Moon S. Control methods of inverter-interfaced distributed generators in a microgrid system. IEEE Trans Ind Appl 2010;46(3):1078–88.
[11] Rokrok E, Golshan MEH. Adaptive voltage droop scheme for voltage source converters in an islanded multibus microgrid. Inst Eng Technol Gen Transm Distrib 2010;4(5):562–78.
[12] Savaghebi M, Jalilian A, Vasquez JC, Guerrero JM. Secondary control scheme for voltage unbalance compensation in an islanded droop controlled microgrid. IEEE Trans Smart Grid 2012;3(2):797–807.
[13] Hojo M, Iwase Y, Funabashi T, Ueda Y. A method of three-phase balancing in microgrid by photovoltaic generation systems. In: Proc EPE-PEMC Conf, 2008. p. 2487–91.
[14] Soultanis NL, Papathanasiou SA, Hatziargyriou ND. A stability algorithm for the dynamic analysis of inverter dominated unbalanced LV microgrids. IEEE Trans Power Syst 2007;22(1):294–304.
[15] Ghazanfari A, Hamzeh M, Mokhtari H. A control method for integrating hybrid power source into an Islanded microgrid through CHB multilevel inverter. In: Proc IEEE PEDSTC Conf, 2013. p. 495–500.
[16] Li Y, Wang M. Control stratories for grid-connected and island dual mode operated inverter under unbalanced grid voltage conditions. In: Proc Conf Rec ICPE ECCE, Harbin, China, 2012. p. 2152–56
[17] Meersman B, Renders B, Degroote L, Vandoorn T, Vandevelde L. The influence of grid-connected three-phase inverters on voltage unbalance. IEEE Power Energy Soc Gen Meeting 2010:1–9.
[18] Yazdani A, Iravani MR. A unified dynamic model and control for the voltage-sourced converter under unbalanced grid conditions. IEEE Trans Power Delivery 2006;21(3):1620–9.
[19] Shang L, Hu J. Sliding-mode-based direct power control of grid-connected wind-turbine-driven doubly fed induction generators under unbalanced grid voltage conditions. IEEE Trans Energy Conv 2012;27(2):362–73.

[20] Shang L, Sun D, Hu J. Sliding-mode-based direct power control of grid-connected voltage-sourced inverters under unbalanced network conditions. IET Power Electron 2011;4(5):570–9.
[21] Delghavi MB, Yazdani A. Islanded-mode control of electronically coupled distributed-resource units under unbalanced and nonlinear load conditions. IEEE Trans Power Del 2011;26(2):661–73.
[22] Hamzeh M, Karimi H, Mokhtari H. A new control strategy for a multi-bus MV microgrid under unbalanced conditions. IEEE Trans Power Syst 2012;27(4):2225–32.
[23] Wang F, Duarte JL, Hendrix MAM. Pliant active and reactive power control for grid-interactive converters under unbalanced voltage dips. IEEE Trans Power Electron 2011;26(5):1511–21.
[24] Suul JA, Luna A, Rodriguez P, Undeland T. Virtual-flux-based voltage-sensorless power control for unbalanced grid conditions. IEEE Trans Power Electron 2012;27(9):4071–87.
[25] Castilla M, Miret J, Sosa JL, Matas J, de Vicuna LG. Grid-fault control scheme for three-phase photovoltaic inverters with adjustable power quality characteristics. IEEE Trans Power Electron 2010;25(12):2930–40.
[26] Zhou Y, Bauer P, Ferreira J, Pierik J. Operation of grid-connected DFIG under unbalanced grid voltage condition. IEEE Trans Energy Conv 2009;24(1):240–6.
[27] Wang F, Duarte J, Hendrix M. High performance stationary frame filters for symmetrical sequences or harmonics separation under a variety of grid conditions. In: Proc. IEEE APEC, 2009. p. 1570–76.
[28] Sallam A, Malik O. Voltage Variations. In: Brown F, editor. Electric Distribution Systems, 1st ed., Wiley-IEEE Press, 2011. p. 319–20.
[29] Vazquez S, Sanchez JA, Reyes R, Leon JI, Carrasco JM. Adaptive vectorial filter for grid synchronization of power converters under unbalanced and/or distorted grid conditions. IEEE Trans Ind Electron 2014;61(3):1355–67.
[30] Slotine JE, Li W. Applied nonlinear control. Englewood Cliffs, NJ: Prentice-Hall; 1991.
[31] Shojaeian S, Soltani J, Markadeh GA. Damping of low frequency oscillations of multi-machine multi-UPFC power systems, based on adaptive input-output feedback linearization control. Power Systems IEEE Trans Power Sys 2012;27(4):1831–40.
[32] Krause PC, Wasynczuk O, Sudhoff S. Analysis of electric machinery and drive systems. In: 2nd ed., Wiley-IEEE Press, 2002. p. 383–84.